PROCEEDINGS of the
23rd International Congress on Acoustics
9 to 13 September 2019 in Aachen, Germany

[Local directional source modeling in wave-based acoustic simulation]

Stefan Bilbao[(1)], Jens Ahrens[(2)], Brian Hamilton[(1)]

[(1)]Acoustics and Audio Group, University of Edinburgh, United Kingdom, sbilbao@ed.ac.uk, brian.hamilton@ed.ac.uk

[(2)]Audio Technology Group, Division of Applied Acoustics, Chalmers University of Technology, Gothenburg, Sweden, jens.ahrens@chalmers.se

Abstract

Time-domain wave-based simulation approaches such as the finite difference time domain (FDTD) method allow for a complete solution to the problem of virtual acoustics over the entire frequency range, in contrast with the methods of geometric acoustics which are valid in the limit of high frequencies. They also allow for flexible modelling of sources and receivers, due to the inherently local nature of the computation, and complete access to the computed acoustic field over an enclosure. In this paper, a method for the emulation of sources of arbitrary directivity is presented, framed directly as an inhomogeneous wave equation. The additional terms in the wave equation take the form of Dirac delta functions and their distributional derivatives, and collections of such terms may be associated directly with an expansion of source directivity in terms of spherical harmonics. The local nature of the model implies a locally-defined efficient computational approach for wave-based methods defined over a spatial grid. Numerical results are presented.

Keywords: virtual acoustics, room acoustics, computational acoustics, source modeling, finite difference time domain

1 INTRODUCTION

Volumetric time-domain wave-based methods for room acoustics and auralisation purposes were proposed in the mid 1990s [12, 22, 8, 9]. In such a simulation framework, the time evolution of acoustic field is modeled in its entirety over the room volume, and the simulation operates as a recursive time-stepping method defined over a spatial grid. Many varieties are available, including the finite difference time domain (FDTD) method [30, 25], finite volume methods [4, 6], and pseudospectral methods [14, 17]. In particular, FDTD methods, defined over regular grids, are equivalent to digital waveguide mesh methods, also proposed for room acoustics simulation [18]. (The term “wave-based" is also used to refer to non-volumetric simulation methods such as the boundary element method (BEM) [29], which often operate in the frequency domain.) Time-domain wave-based methods, which compute an approximate wideband solution to the wave equation over an enclosure, subject to wall conditions and source excitation, can be viewed in contrast with so-called geometrical acoustics (GA) algorithms such as ray tracing [16] or the image source method [2], which represent an approximation to wave-based acoustics in the limit of high frequencies. For audio rate simulation, computational cost is necessarily high, due to the grid density required (of at most 1 cm resolution), but simulation for reasonable-sized spaces is now coming within range of commercially-available hardware such as GPUs [27].

Source modeling, in the setting of time-domain wave-based simulation, has been approached by various authors, usually focusing on omnidirectional, dipole or cardioid source directivities [11, 24, 10, 15, 23, 19]. In some approaches, there have been attempts at calibrating an FDTD scheme against measured source directivity [13, 26]. In almost all cases above, however, a continuous spatio-temporal model of the underlying system is unavailable; sources are implemented in an FDTD scheme through the insertion of driving signals at grid locations. In the interest of greater generality and flexibility, some models of source directivity do employ such a continuous model, framed as the 3D wave equation accompanied by a driving term which has the form of a Dirac delta function under repeated differentiation. A source model of this type corresponding to a multipole expansion has been presented in [5, 3], and allows for a convenient starting point for discretisation, regardless of the particular choice of method.

A better choice, which matches well with typical representations of sources in terms of directivity, is a source model framed directly in terms of spherical harmonics. Such a model is available in a full spatio-temporal form, in which case source directivity is incorporated into the definition of spatial differential operators applied to a Dirac delta function which appears as a driving term. Such a model is presented here, accompanied by simple strategies for discretisation. Numerical results are presented.

2 A SPATIO-TEMPORAL MODEL OF SOURCE DIRECTIVITY

The standard model of wave propagation used in room acoustics is the 3D wave equation:

$$\frac{1}{c^2}\partial_t^2 p - \Delta p = 0\,. \tag{1}$$

Here, $p(\mathbf{x},t)$ represents the acoustic pressure in an enclosure, as a function of coordinate $\mathbf{r} = [x, y, z] \in \mathbb{R}^3$, and $t \in \mathbb{R}$. In this paper, concerned with localised models of sources, the problem is assumed defined in free space, and wall conditions need not be supplied. c is the wave speed, in m/s, ∂_t represents partial differentiation with respect to time t, and Δ is the 3D Laplacian, defined in terms of the 3D gradient operation

$$\nabla = [\partial_x, \partial_y, \partial_z] \tag{2}$$

where ∂_x, ∂_y and ∂_z represent partial derivatives with respect to coordinate x, y and z, respectively.

A model including a source with aribitrary directivity has been presented in [3, 5]. Though presented in a compact tensor form in [5], it may be written in expanded form as

$$\frac{1}{c^2}\partial_t^2 p - \Delta p = \sum_{\eta_x=0}^{\infty}\sum_{\eta_y=0}^{\infty}\sum_{\eta_z=0}^{\infty} \psi_{\eta_x,\eta_y,\eta_z}(t)\,\partial_x^{\eta_x}\partial_y^{\eta_y}\partial_z^{\eta_z}\delta^{(3)}(\mathbf{r}) \tag{3}$$

Here, $\delta^{(3)}(\mathbf{r})$ represents a 3D Dirac delta function selecting the source location at $\mathbf{r} = \mathbf{0}$. Each term, indexed by non-negative integers η_x, η_y, η_z represents the contribution of a single multipole to the corresponding source directivity, and is accompanied by a distinct driving term $\psi_{\eta_x,\eta_y,\eta_z}(t)$. For example, the term with $\eta_x = 0$, $\eta_y = 0$, and $\eta_z = 0$ corresponds, in isolation, to a monopole [20]; that with $\eta_x = 1$, $\eta_y = 0$ and $\eta_z = 0$ to a dipole oriented along the x coordinate, and that with $\eta_x = 0$, $\eta_y = 0$ and $\eta_z = 2$ to a longitudinal quadrupole oriented along the z coordinate.

2.1 Spherical Harmonic Representation

The directivity pattern associated with a given term in (3) is, in general, frequency dependent in a nontrivial way. Each term corresponds, in general, to a frequency-dependent combination of spherical harmonic directivity patterns. To simplify the representation in (3), and render it more suitable for matching against known directivity patterns, a spherical harmonic representation of the source term is of great utility.

To this end, consider the family of real-valued spherical harmonic functions $Y_{l,m}(\boldsymbol{\gamma})$, indexed by integers $l \geq 0$ and $-l \leq m \leq l$. When written as a function of the components of the unit-length 3-vector $\boldsymbol{\gamma} = \mathbf{r}/|\mathbf{r}|$, $Y_{l,m}(\boldsymbol{\gamma})$ is a homogeneous polynomial of degree l. For example, $Y_{0,0} = \sqrt{1/4\pi}$, $Y_{1,-1} = \sqrt{3/4\pi}\gamma_y$, $Y_{2,0} = \sqrt{5/16\pi}\left(2\gamma_z^2 - \gamma_x^2 - \gamma_y^2\right)$. Define now the spatial differential operator $D_{l,m}$ in terms of the gradient operator as defined in (2) as [21, 7]

$$D_{l,m} = Y_{l,m}(\nabla) \qquad \text{or} \qquad D_{l,m} = \sum_{\boldsymbol{\xi}\in\mathbb{V}^l} \sigma_{l,m}^{(\boldsymbol{\xi})} \prod_{\nu=x,y,z} \partial_\nu^{\xi_\nu} \quad , \quad \mathbb{V}^l = \{\mathbf{v} \in \mathbb{Z}_+^3 \,|\, \|\mathbf{v}\|_1 = l\} \tag{4}$$

for some coefficients $\sigma_{l,m}^{(\boldsymbol{\xi})}$. The differential operator $D_{l,m}$ is homogeneous and of degree l. See Table 1.

Table 1. $D_{l,m}$ for $l = 0,1,2,3$ in Cartesian form.

$m \backslash l$	0	1	2	3
-3	·	·	·	$\sqrt{\frac{35}{32\pi}}\left(3\partial_x^2\partial_y - \partial_y^3\right)$
-2	·	·	$\sqrt{\frac{15}{4\pi}}\partial_x\partial_y$	$\sqrt{\frac{105}{4\pi}}\partial_x\partial_y\partial_z$
-1	·	$\sqrt{\frac{3}{4\pi}}\partial_y$	$\sqrt{\frac{15}{4\pi}}\partial_y\partial_z$	$\sqrt{\frac{21}{32\pi}}\left(4\partial_z^2\partial_y - \partial_x^2\partial_y - \partial_y^3\right)$
0	$\sqrt{\frac{1}{4\pi}}$	$\sqrt{\frac{3}{4\pi}}\partial_z$	$\sqrt{\frac{5}{16\pi}}\left(2\partial_z^2 - \partial_x^2 - \partial_y^2\right)$	$\sqrt{\frac{7}{16\pi}}\left(2\partial_z^3 - 3\partial_x^2\partial_z - 3\partial_y^2\partial_z\right)$
1	·	$\sqrt{\frac{3}{4\pi}}\partial_x$	$\sqrt{\frac{15}{4\pi}}\partial_x\partial_z$	$\sqrt{\frac{21}{32\pi}}\left(4\partial_z^2\partial_x - \partial_y^2\partial_x - \partial_x^3\right)$
2	·	·	$\sqrt{\frac{15}{16\pi}}\left(\partial_x^2 - \partial_y^2\right)$	$\sqrt{\frac{105}{16\pi}}\left(\partial_x^2\partial_z - 3\partial_y^2\partial_z\right)$
3	·	·	·	$\sqrt{\frac{35}{32\pi}}\left(\partial_x^3 - 3\partial_y^2\partial_x\right)$

An alternative representation for (3) is

$$\frac{1}{c^2}\partial_t^2 p - \Delta p = \sum_{l=0}^{\infty}\sum_{m=-l}^{l} c^l f_{l,m}(t) D_{l,m}\delta^{(3)}(\mathbf{r}) \qquad f_{l,m} = a_{l,m} * f \tag{5}$$

Here, the driving signals $f_{l,m}(t)$ are assumed related to an underlying scalar driving function $f(t)$ through a filtering operation, where $*$ indicates convolution. The filter responses $a_{l,m}(t)$ completely determine the directivity of the source model, as will be shown below.

2.2 Solutions

Consider the basic equation describing a monopole source:

$$\frac{1}{c^2}\partial_t^2 p - \Delta p = f(t)\delta^{(3)}(\mathbf{r}) \tag{6}$$

The well-known solution $p(\mathbf{r},t)$ and its Fourier transform $\hat{p}(\mathbf{r},\omega)$, for angular frequency ω (using the sign convention of Williams [28]) are

$$p(\mathbf{r},t) = \frac{f(t-r/c)}{4\pi r} \qquad \hat{p}(\mathbf{r},\omega) = \frac{\hat{f}e^{i\omega r/c}}{4\pi r} = \frac{i\omega}{4\pi c}\hat{f}h_0^{(1)}(\omega r/c) \tag{7}$$

where $r = |\mathbf{r}|$, and where $\hat{f}(\omega)$ is the Fourier tranform of $f(t)$. $h_0^{(1)}$ is the zeroth order spherical Hankel function of the first kind.

Through superposition, the solution to (5) is then

$$p(\mathbf{r},t) = \sum_{l=0}^{\infty}\sum_{m=-l}^{l} c^l f_{l,m}(t) D_{l,m}\left(\frac{f_{l,m}(t-r/c)}{4\pi r}\right) \qquad \hat{p}(\mathbf{r},\omega) = \frac{i\omega}{4\pi c}\hat{f}\sum_{l=0}^{\infty}\sum_{m=-l}^{l} c^l \hat{a}_{l,m}(\omega) D_{l,m}h_0^{(1)}(\omega r/c) \tag{8}$$

where $\hat{f}_{l,m}(\omega) = \hat{f}(\omega)\hat{a}_{l,m}(\omega)$. Using the identity (not proven here):

$$D_{l,m}h_0^{(1)}(\omega r/c) = (-\omega/c)^l Y_{l,m}(\boldsymbol{\gamma}) h_l^{(1)}(\omega r/c) \tag{9}$$

where $h_l^{(1)}$ is the lth order spherical Hankel function of the first kind leads to the following frequency domain expression for the solution $\hat{p}(\mathbf{r},\omega)$:

$$\hat{p} = \frac{i\omega}{4\pi c}\hat{f}\sum_{l=0}^{\infty}\sum_{m=-l}^{l} (-\omega)^l \hat{a}_{l,m}(\omega) Y_{l,m}(\boldsymbol{\gamma}) h_l^{(1)}(\omega r/c)\,. \tag{10}$$

Dividing by the response $\hat{f}$ of the source signal leaves an expression for the directivity which recovers the standard form for the exterior field of a source—see, e.g., [1]. The model (5), however, is expressed entirely in the spatio-temporal domain, and is a good candidate for discretisation through volumetric wave-based methods of any type—note that, as yet, no discretisation has been employed.

2.3 Displaced Monopole

An interesting test case is that of the monopole source located at coordinates $\mathbf{r} = \mathbf{r}_0$, where $\mathbf{r}_0 = r_0 \boldsymbol{\gamma}_0$, for a displacement distance r_0 and unit-length direction vector $\boldsymbol{\gamma}_0$:

$$\frac{1}{c^2}\partial_t^2 p - \Delta p = f(t)\delta^{(3)}(\mathbf{r} - \mathbf{r}_0) \tag{11}$$

In this case, an analytic time domain expression for the filters $a_{l,m}(t)$ (necessarily non-causal) in model (5) is available:

$$a_{l,m}(t) = 4\pi(-1)^l Y_{l,m}(\boldsymbol{\gamma}_0)\frac{t_0^{l-1}}{2\cdot(2l)!!}\left(1-\frac{t^2}{t_0^2}\right)^l \sqcap(t/t_0) \qquad \text{where} \qquad \sqcap(\xi) = \begin{cases} 1, & |\xi| \le 1 \\ 0, & |\xi| > 1 \end{cases} \qquad t_0 = r_0/c \tag{12}$$

3 FDTD METHODS

Only the most basic FDTD scheme, sometimes referred to as the seven-point scheme, will be described here. But the method described below can be applied to any volumetric time-domain method.

Consider a grid function $p_{\mathbf{q}}^n$, indexed by integer $\mathbf{q} \in \mathbb{Z}^3$ and $n \in \mathbb{Z}$. $p_{\mathbf{q}}^n$ represents an approximation to $p(\mathbf{r},t)$ at $t = nT$ and $\mathbf{x} = \mathbf{q}X$. Here, T is the time step, in s (and $1/T$ is the sample rate), and X is the grid spacing, in m. The simplest possible FDTD scheme for the general system (5) is

$$p_{\mathbf{q}}^{n+1} = 2p_{\mathbf{q}}^n - p_{\mathbf{q}}^{n-1} + \lambda^2 \sum_{\mathbf{e}\in\mathbb{Q}}\left(p_{\mathbf{q}+\mathbf{e}}^n - p_{\mathbf{q}}^n\right) + T^2 \sum_{l=0}^{\infty}\sum_{m=-l}^{l} c^{2+l} f_{l,m}^n d_{l,m} s_{\mathbf{q}} \quad , \quad \mathbb{Q} = \{\mathbf{e} \in \mathbb{Z}^3 | \|\mathbf{e}\|_1 = 1\} \quad , \quad \lambda = cT/X \tag{13}$$

The constant λ is referred to as the Courant number for the scheme, and is bounded by $\lambda \le 1/\sqrt{3}$ for numerical stability. $s_{\mathbf{q}}$ is an approximation to the 3D Dirac delta function, and defined as

$$s_{\mathbf{q}} = \begin{cases} 1/X^3, & \mathbf{q} = \mathbf{0} \\ 0, & \text{otherwise} \end{cases} . \tag{14}$$

The time series $f_{l,m}^n$ result from discrete time convolution between the driving function f^n and the individual spherical harmonic channel filters $a_{l,m}^n$, both assumed known *a priori*. The discrete operators $d_{l,m}$ are approximations to the partial differential operators $D_{l,m}$, and their construction is described below.

3.1 Discrete Spherical Harmonic Operators

Approximations to the operators $D_{l,m}$, as defined in (4) may be obtained by various means—see, e.g., [5]. A basic approach is through standard difference operations. Consider a grid function $g_{\mathbf{q}}$, defined for $\mathbf{q} \in \mathbb{Z}^3$. Difference operators d_ν^+ and d_ν^-, approximating ∂_ν, and an averaging operator μ_ν^- may be defined as

$$d_\nu^+ g_{\mathbf{q}} = \frac{1}{X}\left(g_{\mathbf{q}+\mathbf{e}_\nu} - g_{\mathbf{q}}\right) \qquad d_\nu^- = \frac{1}{X}\left(g_{\mathbf{q}} - g_{\mathbf{q}-\mathbf{e}_\nu}\right) \qquad \mu_\nu^- = \frac{1}{2}\left(g_{\mathbf{q}} + g_{\mathbf{q}-\mathbf{e}_\nu}\right). \tag{15}$$

Here $\mathbf{e}_\nu$ is a unit vector in direction ν.

Consider now the approximation of ∂_ν^ξ, a ξth spatial derivative in coordinate ν; ξ may be decomposed uniquely as $\xi = 2M_\xi + \alpha_\xi$ for integer $M_\xi \ge 0$ and $\alpha_\xi \in \{0,1\}$. A centered approximation d_ν^ξ follows as

$$d_\nu^\xi \triangleq \left(\mu_\nu^-\right)^{\alpha_\xi}\left(d_\nu^+\right)^{M_\xi+\alpha_\xi}\left(d_\nu^-\right)^{M_\xi} \approxeq \partial_\nu^\xi , \tag{16}$$

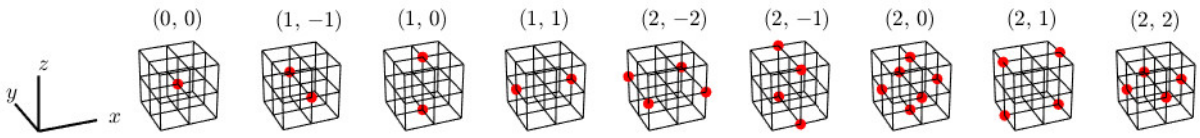

Figure 1. Stencils of the discrete operators $d_{l,m}$, for $l = 0, 1, 2..$

Using the expanded representation of $D_{l,m}$ from (4), one may then arrive at a centered approximation $d_{l,m}$ to $D_{l,m}$:

$$d_{l,m} = \sum_{\boldsymbol{\xi} \in \mathbb{V}^l} \sigma_{l,m}^{(\boldsymbol{\xi})} \prod_{\nu=x,y,z} d_\nu^{\xi_\nu} \approx D_{l,m} \,. \tag{17}$$

See Figure 1 for a graphical representation of the operators $d_{l,m}$.

4 SIMULATION RESULTS

In this section, some basic results are shown, using scheme (13), operating at 44.1 kHz, over a cube of side length 2 m.

As a first step, it is useful to regenerate spherical harmonic directivity patterns by exciting only one of the channels (i.e., setting all filters $a_{l,m}$ to zero except for one in the scheme (13)). The scheme is excited by setting f^n to a unit impulse, and then drawing output from a set of receivers located on a sphere of radius 0.3 m around the source location. High-order separable interpolating approximants are used [5] for the receivers (60 azimuthal by 30 in inclination). The resulting outputs are Fourier-transformed, and directivity magnitude is as shown in Figure 2 at 2 kHz, for all spherical harmonics up to $l = 3$.

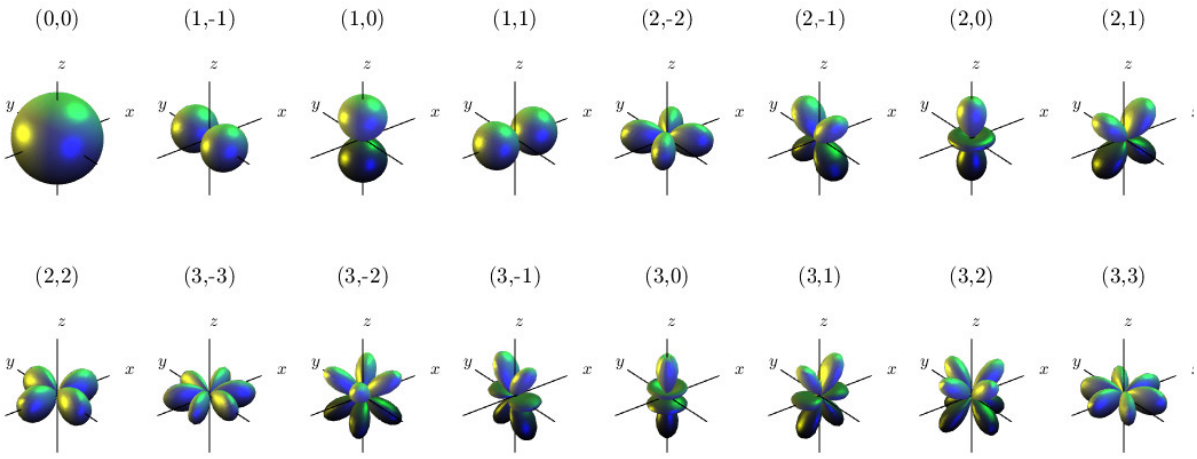

Figure 2. Spherical harmonic directivity patterns generated using scheme (13) at 44.1 kHz.

As a second example, consider the case of the displaced monopole source, as described in Section 2.3. Here, the excitation f^n is chosen as a Gaussian function, of variance $\sigma = 2 \times 10^{-4}$ s, and the displaced source location is chosen as $\mathbf{r}_0 = [-0.2, 0, 0]$. The filters $a_{l,m}^n$ are sampled from the exact expressions given in (12). Snapshots of

the time evolution of the acoustic field are as shown in Figure 3, for different choices of the maximal spherical harmonic order L.

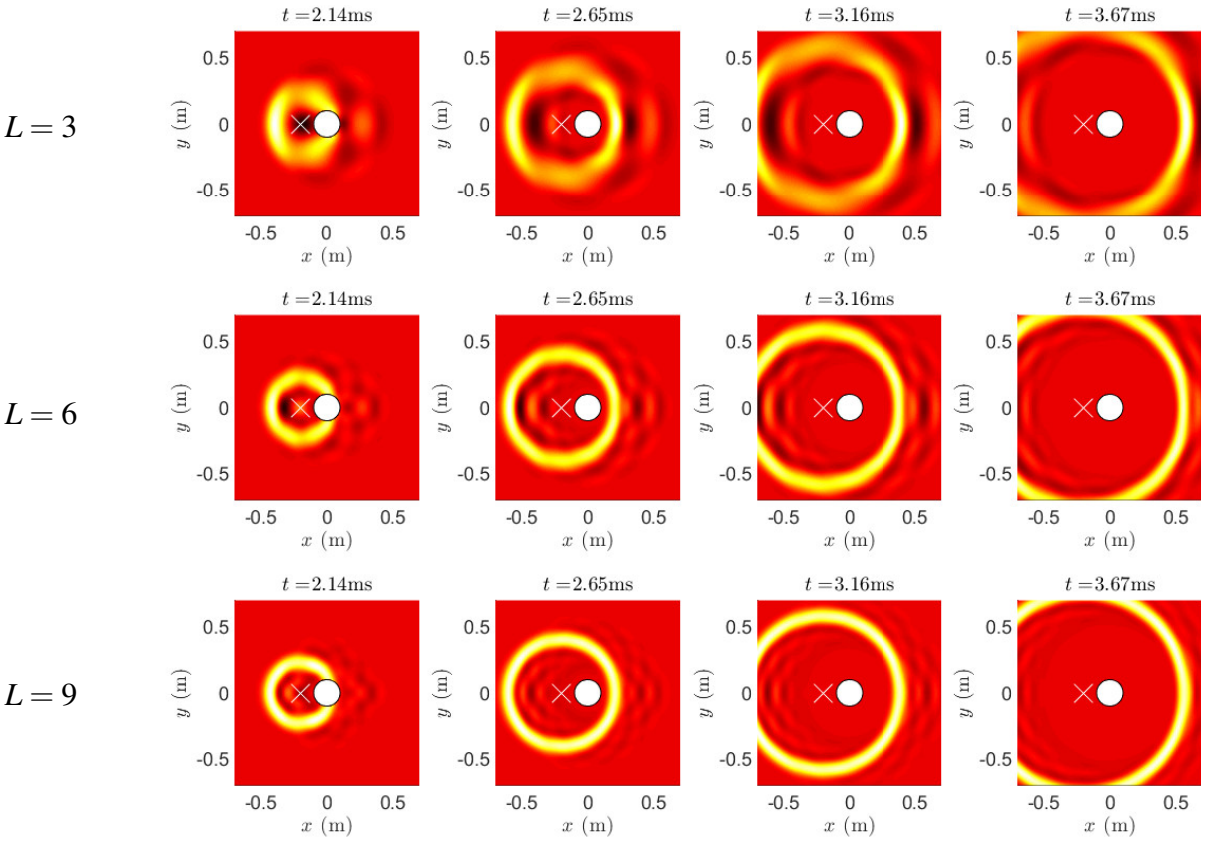

Figure 3. Snapshots of the time evolution of the acoustic field in the case of a displaced monopole. The driving term for the FDTD scheme is located within the white circle, and the location of the displaced source is indicated by a $\times$ symbol. Results are shown for a maximal spherical harmonic order of $l \leq L$, for $L = 3$ (top row), $L = 6$ (middle row) and $L = 9$ (bottom row).

5 CONCLUDING REMARKS

A basic model of source directivity has been presented here, intended for use within a volumetric wave-based simulation framework. As such, the model is expressed entirely in the spatio-temporal domain, as an extension of the 3D wave equation. Such a model lends itself easily to a time stepping method defined over a regular Cartesian grid, as presented here, but the model in (5) does not require this. Operation over unstructured grids is also possible, requiring some approximation to the derivatives of the Dirac distribution. As with all wave-based methods, such a model naturally reproduces near-field effects.

Regardless of the particular discretisation method, however, an important feature is that the approximation to the source is local, and thus not computationally costly. Indeed, for the simulation scenario presented here, the computational cost associated with the incorporation of a source term in the scheme (13) is far less than the cost of the operation of the scheme over the problem interior. Such a localised source model is also flexible, in the sense that it may be placed independently of any consideration of room boundary conditions, and also that, once the appropriate filters $a^n_{l,m}$ and spatial difference operators have been determined, the source location

may be displaced within the simulation volume without any additional computation. In addition, fitting of the filters $a_{l,m}$ against measured directivity patterns may be carried out independently of the particular choice of time stepping scheme.

REFERENCES

[1] J. Ahrens. *Analytic Methods of Sound Field Synthesis*. Springer, Heidelberg, Germany, 2012.

[2] J. Allen and D. Berkley. Image method for efficiently simulating small-room acoustics. *J. Acoust. Soc. Am.*, 66(4):943–950, 1979.

[3] M. Bencomo and W. Symes. Discretization of multipole sources in a finite difference setting for wave propagation problems. *J. Comp. Phys.*, 386:296 – 322, 2019.

[4] S. Bilbao. Modeling of complex geometries and boundary conditions in finite difference/finite volume time domain room acoustics simulation. *IEEE Trans. Audio Speech Language Proces.*, 21(7):1524–1533, 2013.

[5] S. Bilbao and B. Hamilton. Directional sources in wave-based acoustic simulation. *IEEE Trans. Audio Speech Language Proces.*, 27:415–428, 2019.

[6] S. Bilbao, B. Hamilton, J. Botts, and L. Savioja. Finite volume time domain room acoustics simulation under general impedance boundary conditions. *IEEE/ACM Trans. Audio Speech Language Proces.*, 24(1):161–173, 2016.

[7] S. Bilbao, A. Politis, and B. Hamilton. Local time-domain spherical harmonic spatial encoding for wave-based acoustic simulation. *IEEE Signal Proces. Lett.*, 26(4):617–621, 2019.

[8] D. Botteldooren. Acoustical finite-difference time-domain simulation in a quasi-cartesian grid. *J. Acoust. Soc. Am.*, 95(5):2313–2319, 1994.

[9] D. Botteldooren. Finite-difference time-domain simulation of low-frequency room acoustic problems. *J. Acoust. Soc. Am.*, 98(6):3302–3308, 1995.

[10] J. Botts, A. Bockman, and N. Xiang. On the selection and implementation of sources for finite-difference methods. In *Proc. 20th Int. Congr. Acoust.*, Sydney, Australia, 2010.

[11] A. Celestinos and S. Nielsen. Low-frequency loudspeaker room simulation using finite differences in the time domain part 1: Analysis. *J. Audio Eng. Soc.*, 56(10):772–786, 2008.

[12] O. Chiba, T. Kashiwa, H. Shimoda, S. Kagami, and I. Fukai. Analysis of sound fields in three dimensional space by the time-dependent finite-difference method based on the leap frog algorithm. *J. Acoust. Soc. Jpn.(J)*, 49:551–562, 1993.

[13] J. Escolano, J. Lopez, and B. Pueo. Directive sources in acoustic discrete-time domain simulations based on directivity diagrams. *JASA Express Lett.*, 121:256–262, 2007.

[14] M. Hornikx, W. De Roeck, and W. Desmet. A multi-domain Fourier pseudospectral time-domain method for the linearized Euler equations. *J. Comp. Phys.*, 231(14):4759–4774, 2012.

[15] H. Jeong and L. Y. Source implementation to eliminate low-frequency artifacts in finite difference time domain room acoustic simulation. *J. Acoust. Soc. Am.*, 258–268(1):1112–1118, 2012.

[16] A. Krokstad, S. Strom, and S. Sorsdal. Calculating the acoustical room response by the use of a ray tracing technique. *J. Sound Vib.*, 8(1):118–125, 1968.

[17] R. Mehra, N. Raghuvanshi, L. Savioja, M. Lin, and D. Manocha. An efficient GPU-based time domain solver for the acoustic wave equation. *Appl. Acoust.*, 73(2):83–94, 2012.

[18] D. Murphy, A. Kelloniemi, J. Mullen, and S. Shelley. Acoustic modelling using the digital waveguide mesh. *IEEE Sig. Proc. Mag.*, 24(2):55–66, 2007.

[19] D. Murphy, A. Southern, and L. Savioja. Source excitation strategies for obtaining impulse responses in finite difference time domain room acoustics simulation. *Appl. Acoust.*, 82:6–14, 2014.

[20] A. Pierce. *Acoustics: An introduction to its physical principles and applications*. Acoustical Society of America, 1991.

[21] E. Rowe. Spherical delta functions and multipole expansions. *J. Math. Phys.*, 19:1962–1968, 1978.

[22] L. Savioja, T. Rinne, and T. Takala. Simulation of room acoustics with a 3-D finite-difference mesh. In *Proc. Int. Comp. Music Conf.*, pages 463–466, Århus, Denmark, sep 1994.

[23] J. Sheaffer, M. van Walstijn, and B. Fazenda. Physical and numerical constraints in source modeling for finite difference simulation of room acoustics. *J. Acoust. Soc. Am.*, 135(1), 2014.

[24] A. Southern and D. Murphy. Low complexity directional sound sources for finite difference time domain room acoustic models. In *Proc. 126th Audio Eng. Soc. Conv.*, Munich, Germany, 2009.

[25] J. Strikwerda. *Finite Difference Schemes and Partial Differential Equations*. Wadsworth and Brooks/Cole Advanced Books and Software, Pacific Grove, California, 1989.

[26] D. Takeuchi, K. yatabe, and Y. Oikawa. Source directivity approximation for finite-difference time-domain simulation by estimating initial value. *J. Acoust. Soc. Am.*, 145(4):2638–2649, April 2019.

[27] C. J. Webb and S. Bilbao. Computing room acoustics with CUDA - 3D FDTD schemes with boundary losses and viscosity. In *Proc. IEEE Int. Conf. Acoust., Speech Signal Proces.*, pages 317–320, 2011.

[28] E. Williams. *Fourier Acoustics: Sound Radiation and Nearfield Acoustical Holography*. Academic Press, New York, 1999.

[29] Y. Yasuda and T. Sakuma. Boundary element method. In T. Sakuma, S. Sakamoto, and T. Otsuru, editors, *Computational Simulation in Architectural and Environmental Acoustics*, page 80. Springer, 2014.

[30] K. Yee. Numerical solution of initial boundary value problems involving Maxwell's equations in isotropic media. *IEEE Trans. Antennas Propagation*, 14:302–307, 1966.